JOURNAL OF APPLIED ELECTROCHEMISTRY 26 (1996) 733–740

Characterization of electroless Ni–Mo–P/SnO_2/Ti electrodes for oxygen evolution in alkaline solution

Y. L. LO, S. C. CHOU, B. J. HWANG*

Department of Chemical Engineering, National Taiwan Institute of Technology, Taipei, Taiwan, 10672, Republic of China

Received 10 January 1995; revised 18 December 1995

Ni–Mo–P alloy electrodes, prepared by electroless plating, were characterized for application to oxygen evolution. The rate constants were estimated for oxygen evolution on electrodes prepared at various Mo-complex concentrations. The surface area and the crystallinity increase with increasing Mo content. The electrochemical characteristics of the electrodes were identified in relation to morphology and the structure of the surface. The results show that the electroless Ni–Mo–P electrode prepared at a Mo-complex concentration of 0.01 M provided the best electrocatalytic activity for oxygen evolution.

List of symbols

b	Tafel slope ($mV\,dec^{-1}$)
b'	$\alpha F/RT$ (mV^{-1})
F	Faraday constant ($96\,500\,C\,mol^{-1}$)
j	current density ($mA\,cm^{-2}$)
k'_1	reaction rate of Reaction 1, ($mol^{-1}\,cm^3\,s^{-1}$)
k_1	$= k'_1\gamma C_{OH^-}$ ($mol\,cm^{-2}\,s^{-1}$)
k_{10}	rate constant of Reaction 1 at $\eta = 0$ ($mol\,cm^{-2}\,s^{-1}$)
k'_{c1}	rate constant of Reaction 2 ($mol^{-1}\,cm^3\,s^{-1}$)
k_{c1}	$= k'_{c1}\gamma C_{H_2O}$ ($mol\,cm^{-2}\,s^{-1}$)
k'_{c2}	rate constant of chemical Reaction 3 ($mol^{-1}\,cm^2\,s^{-1}$)
k_{c2}	$= k'_{c2}\gamma^2$ ($mol\,cm^{-2}\,s^{-1}$)
k'_{c3}	rate constant of Reaction 4 ($mol^{-1}\,cm^2\,s^{-1}$)
Q_a	anodic capacity (mC)
Q_c	cathodic capacity (mC)
R	gas constant ($8.314\,J\,mol^{-1}\,K^{-1}$)
R_{ct}	charge transfer resistance ($\Omega\,cm^2$)
R_{ads}	charge transfer resistance due to adsorption effect ($\Omega\,cm^2$)
C_{dl}	double layer capacity ($mF\,cm^{-2}$)
C_{ads}	double layer capacity due to adsorption effect ($mF\,cm^{-2}$)
T	temperature (K)

Greek symbols

α	anodic transfer coefficient
η_{O_2}	oxygen overpotential (mV)
γ	saturation concentration of surface oxide on nickel ($mol\,cm^{-2}$)

1. Introduction

An electrode material must have good electrocatalytic activity and stability. Nickel is an economically feasible material with high electrocatalytic activity for gas evolution [1–6] and organic electrooxidation [7–11]. However, the service life of nickel electrodes still requires improvement. Improvements made by alloying nickel with elements such as iridium and ruthenium [2] have been reported in the literature. Electroless deposition is a promising technique for the manufacture of such electrodes to prepare deposits with desirable characteristics by controlling bath compositions, as well as operating conditions [12–14]. Molybdenum is usually added to Ni-based alloys or steels to improve the corrosion resistance [15–17]. The codeposition of molybdenum with Ni–P films has been employed for improving the thermal stability in view of their application to thin-film resistors [12, 14, 18–20]. On the other hand, Ni–Mo alloy is a kind of Raney nickel with high electrocatalytic activity for hydrogen evolution [21–25] and organic electroreduction [26]. Compared with Ni–Zn, Ni–Co, Ni–W, Ni–Fe and Ni–Cr, Ni–Mo alloy is the best electrocatalyst for hydrogen evolution in alkaline solution [22]. Oxygen evolution is an important reaction in the electrolysis of water, in electrosynthesis and in other processes where oxygen is anodically produced. However, no study on Ni–Mo alloy has been found in the literature for oxygen evolution. In this work the characteristics of Ni–Mo–P electrodes prepared by electroless deposition are investigated. The electrocatalytic activity of electrodes prepared with varying Mo-complex concentrations in the deposition bath has been studied by employing the electrodes for oxygen evolution in 1 M KOH. Scanning electron micrographs (SEM) of the electrode surfaces were also taken. The kinetic parameters were estimated from a comparison of the experimental polarization curves with a kinetic model. The electrocatalytic activities of the electroless Ni–Mo–P electrodes were evaluated by comparison of the rate constants and Tafel slopes. The charge transfer

*To whom correspondence should be addressed.

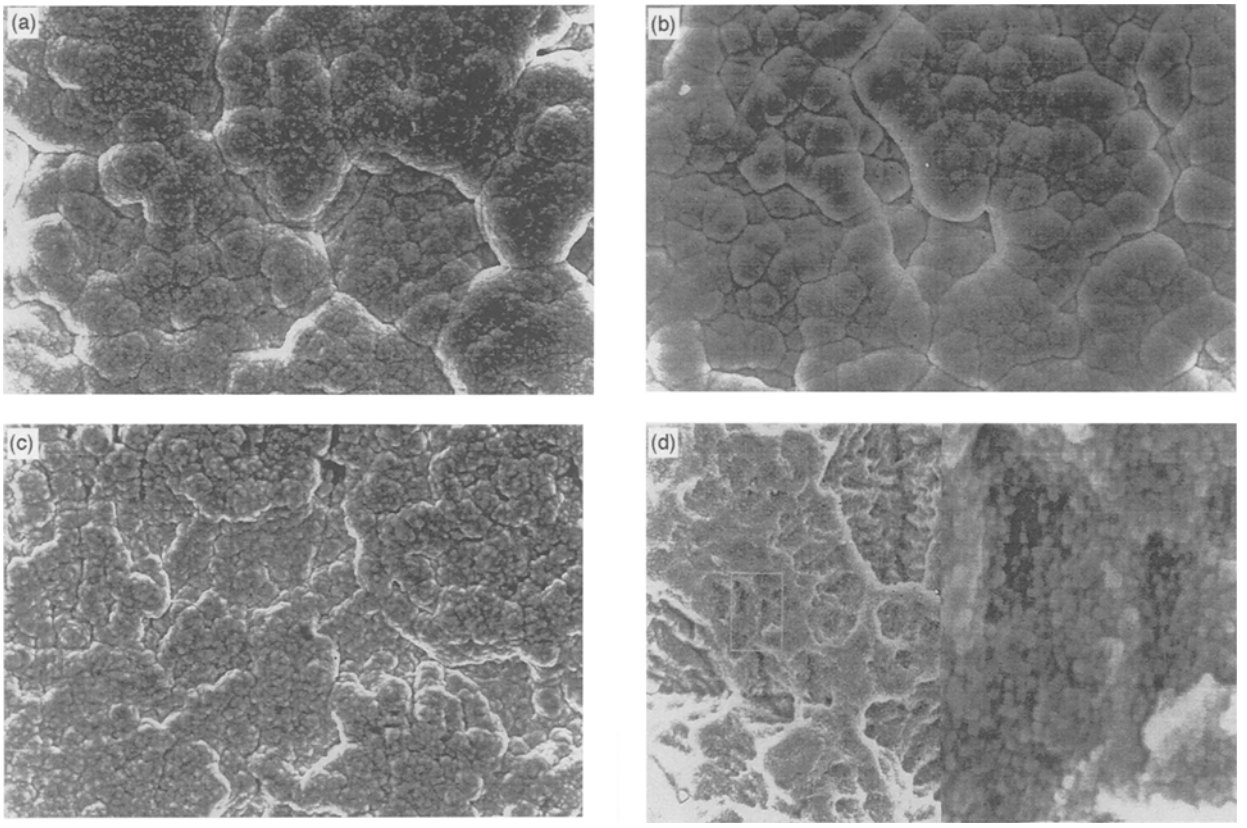

Fig. 1. SEM micrographs of electroless Ni–Mo–P electrodes: (a) M0, (b) M1, (c) M2, (d) M3.

resistances were obtained from a.c.-impedance analysis during water electrolysis. The activity was also characterized in relation to the morphology and structure.

2. Experimental details

Ni–Mo–P deposits were formed by electroless deposition on tin dioxide-coated titanium sheets (20 mm × 25 mm × 0.5 mm) [11]. The substrate was consequently SnO_2/Ti. Due to the SnO_2 layer, titanium oxide formation on the substrate is avoided. Moreover, this layer improves the adhesion of deposits to the substrate. The experimental details of the titanium treatment procedures are described in [6, 11].

The substrates were sensitized in a solution of 1 g $SnCl_2$ and 1 ml HCl in 1 dm^3 for 5 min. The substrates were then activated in a solution of 1 g $PdCl_2$ and 1 ml HCl in 1 dm^3 for 5 min. After pretreatment, electroless Ni–Mo–P electrodes were prepared from a solution of 1 dm^3 containing of 0.1 mol $NiSO_4$, 0.2 mol NaH_2PO_2 0.1 mol Na-citrate, 0.2 mol $CH_2(OH)$-COOH and $0 \sim 0.01$ mol Na_2MoO_4 at pH 9.0 (adjusted by NaOH). 2 ppm $PbNO_3$ was added to the solution as a stabilizer. The bath temperature was maintained at 90 °C. Agitation at 500 rpm was provided by a paired-stirrer thermostat (Eyela ps-60). The water used for solution preparation was redistilled and purified in a NANO pure-II system (Barnstead). All chemicals were of reagent grade without further purification.

The electrochemical experiments were carried out in a three-electrode glass cell with a saturated silver chloride reference electrode (Ag/AgCl). The counter electrode was a platinum electrode. The electrolyte was 1 M KOH and the solution was prepared from analytical grade potassium hydroxide (Janssen Chemica). The solution was deoxygenated by purging with nitrogen gas before each experiment. The working area of the electroless Ni–Mo–P/SnO_2/Ti electrodes was 0.25 cm^2.

Table 1. Some physical characteristics for the electrodes

Electrode	*Average particle size (by SEM)*/μm	*Composition*			*Crystal size* (by XRD)/nm	*Ni(111)/Ni(200)*
		Ni/wt%	*Mo*/wt %	*P*/wt %		
M0	0.67	88.2	0	11.80	1.89	0.11
M1	5.0	84.36	2.21	13.43	1.71	0.17
M2	1.17	85.58	11.08	3.34	14.50	0.45
M3	0.28	83.07	14.37	2.56	18.31	2.92

Polarization curves and the cyclic voltammograms were recorded using a PAR model-273A system. For polarization measurements, rotating disc electrodes were used, while planar electrodes were employed in the cyclic voltammetry. The rotating disk electrodes were prepared by gluing electroless Ni–Mo–P/SnO_2/Ti sheets to a stainless steel rod by conductive gel. The rod was mounted in PTFE. Rotation speed was controlled at 1500 rpm by a Pine 101 rotator. The a.c.- impedance was measured with a Schlumberger SI 1286 + 1260 system. A small-amplitude (10 mV) sine wave was imposed on the electrochemical system. A d.c. bias was set at 500 mV vs Ag/AgCl. Frequency was swept from 65 kHz to 3 mHz. All measurements were done at 30 °C.

The surface morphology of the prepared Ni–Mo–P electrodes was investigated by scanning electron microscopy (Cambridge S360). The structure of the electrodes was studied by X-ray diffraction (Philips PW1710). The spectra were recorded in the interval of 2θ between 20° and 90°. Nickel filtered CuK_α radiation ($\lambda = 0.154\,18$ nm) was used.

3. Results and discussion

3.1. *Physical characteristics of the electroless Ni–Mo–P electrode*

Figure 1 shows micrographs of the electroless Ni–Mo–P electrodes prepared in various Mo^{6+} concentrations (Mo-complex concentrations). The average particle size for the electrodes was estimated from the micrographs and is presented in Table 1. The particle size of the electroless Ni–Mo–P decreases with increasing Mo-complex concentration. The electrode prepared in Mo-complex concentrations of 0, 0.001, 0.005 and 0.01 M is referred to as the M0, M1, M2 and M3 electrode, respectively. The particle size of the M3 electrode is the smallest among the electrodes. The amount of molybdenum alters the morphology of the electroless Ni–Mo–P deposits. The composition of the deposits as analysed by EDS is also listed in Table 2. The molybdenum content increases with increasing Mo-complex concentration while the phosphorus content decreases. X-ray diffraction (XRD) patterns of the electrodes prepared in various Mo-complex concentrations are demonstrated in Fig. 2 (a)–(d). The crystal size was estimated on the basis of the broad peak of Ni(2 0 0) according to the Scheffer formula [27]. The results are reported in Table 1. The crystal size and the crystallinity increase with Mo content. The structure of the Ni–P (M0) electrode is amorphous (microcrystalline state) due to a high phosphor content [13, 19]. Both the peaks, Ni(1 1 1) and Ni(2 0 0) planes, are obvious and the intensity ratio of Ni(1 1 1)/Ni(2 0 0) increases with Mo content. The ratio for the M3 electrode is much larger than unity. Previous literature showed that electrocatalytic activity of nickel came from Ni(1 1 1) rather than Ni(2 0 0) [28]. This means that the electrocatalytic activity of Ni(1 1 1) is larger than that of

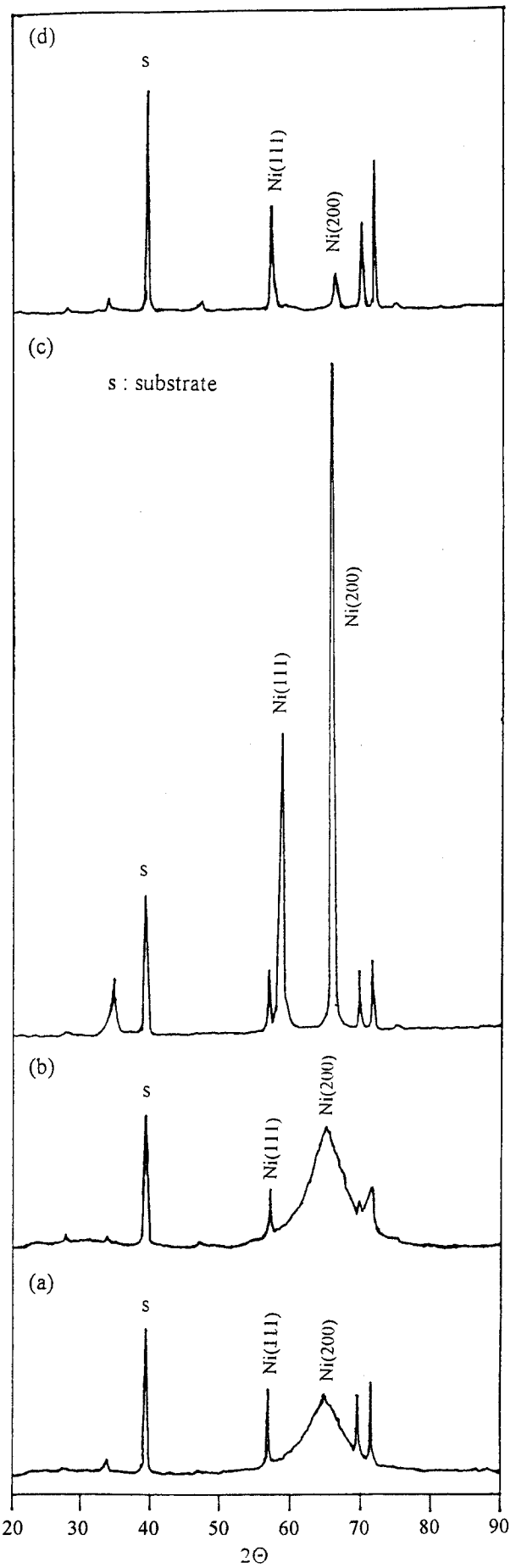

Fig. 2. XRD patterns of electroless Ni–Mo–P electrodes: (a) M0, (b) M1, (c) M2, (d) M3. (s = substrate).

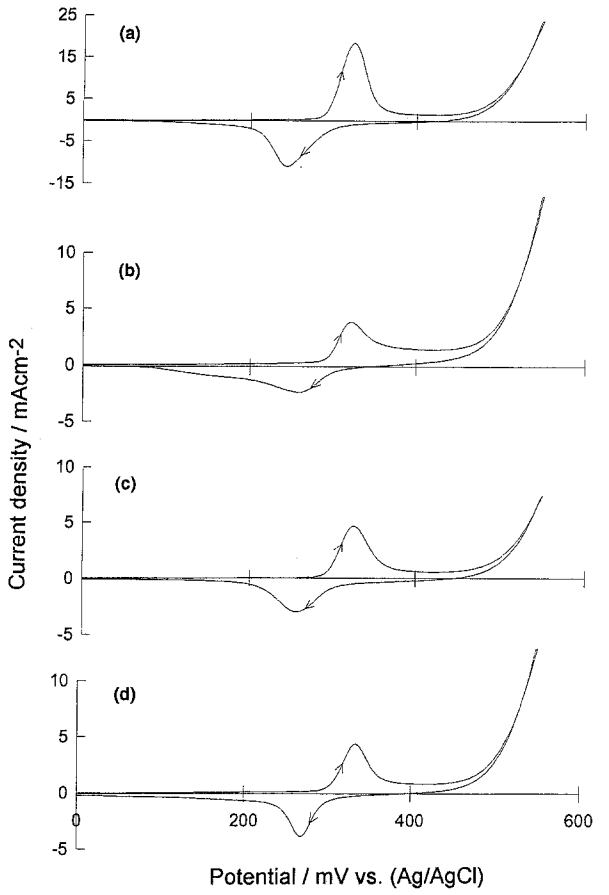

Fig. 3. Cyclic voltammograms of the electroless Ni–Mo–P electrodes in 1 M KOH, scan rate 50 mV s^{-1}, 30 °C. (a) M0, (b) M1, (c) M2, (d) M3.

Ni(2 0 0). Whether the electrocatalytic activity of the electroless Ni–Mo–P relates to the ratio of Ni(1 1 1)/Ni(2 0 0) is currently under investigation.

3.2. *Electrochemical characteristics of the electroless Ni–Mo–P electrodes*

3.2.1. Cyclic voltammograms and steady state polarization curves. The cyclic voltammograms of the electroless Ni–P and Ni–Mo–P electrodes prepared in various Mo-complex concentrations are illustrated in Fig. 3. Fig. 3(a) shows the voltammogram of the electroless Ni–P electrode in 1 M KOH solution. This result is similar to a typical result for the nickel electrode involving a redox pair, $Ni(OH)_2$/NiOOH [1, 6, 11], indicating that the electrocatalytic activity of the Ni–Mo–P electrode derives from the nickel component. During the anodic scan, nickel hydroxide is first oxidized to nickel oxyhydroxide and then oxygen evolves [1]. The cathodic peak arises from the reduction of nickel oxyhydroxide to nickel hydroxide in the cathodic scan. Figure 4 demonstrates the j/E curves of different electrodes at a scan rate of 0.1 mV s^{-1}. The scan rate was chosen so steady state polarization curves could be obtained. The reaction rate constants were estimated from the j/E relationship. The methodology was introduced in previous studies [6, 11] and was employed in this work to evaluate kinetic parameters of oxygen

Table 2. Electrochemical characteristic parameters for the electroless Ni–Mo–P electrodes

Electrode	η_{O_2}/mV (17.5 mA cm^{-2})	η_{O_2}/mV (100 mA cm^{-2})	Q_c/Q_a
0	371	577	0.954
M1	396	592	0.860
M2	381	583	0.916
M3	365	556	0.999

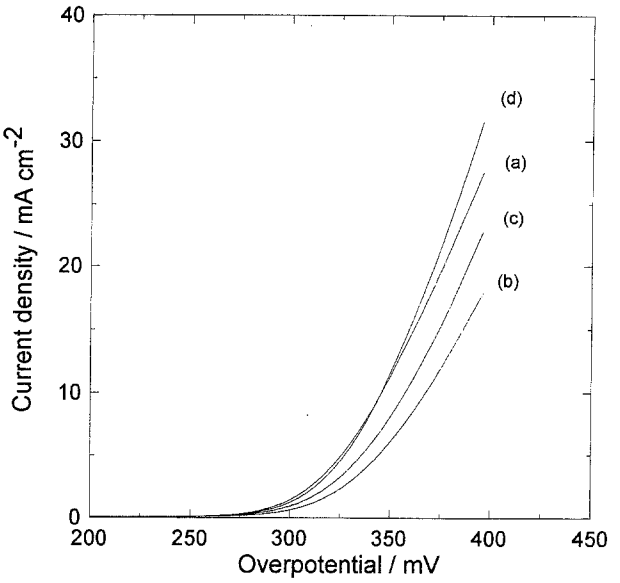

Fig. 4. j/E curves on the electroless Ni–Mo–P electrodes in 1 M KOH, scan rate 0.1 MV s^{-1}, 30 °C. (a) M0, (b) M1, (c) M2, (d) M3.

evolution on the Ni–Mo–P electrodes. The overpotentials for oxygen evolution on the electrodes are shown in Table 2. The overpotential first increases with the introduction of Mo component and then decreases at the M3 electrode. For the M3 electrode, the overpotential is close to that for the Ni–P (M0) electrode at lower current density (j = 17.5 mA cm^{-2}). However, the overpotential for the M3 electrode is lower than that for the M0 at 100 mA cm^{-2}. In the XRD results, the ratio of Ni(1 1 1)/Ni(2 0 0) of the M3 electrode is the largest. The overpotential of the M3 electrode is the lowest. This indicates that the electrocatalytic activity of the Ni–Mo–P electrode relates to its structure and mainly to the intensity ratio of the crystalline planes, Ni(1 1 1) to Ni(2 0 0). The electroless Ni–P electrode possesses better activity than the Ni–Mo–P electrodes at current density less than 10 mA cm^{-2}, as shown in Fig. 4. This possibly arises from the amorphous structure of the electroless Ni–P deposit. From previous investigations [29, 30], active sites are more dispersed on the surface of the electrode with an amorphous structure. At low current density, the electroless Ni–P electrode possesses better electrocatalytic activity due to uniform active site dispersion. With the introduction of molybdenum, the crystallinity increases and the ratio of Ni(1 1 1)/Ni(2 0 0) varies with Mo content. The

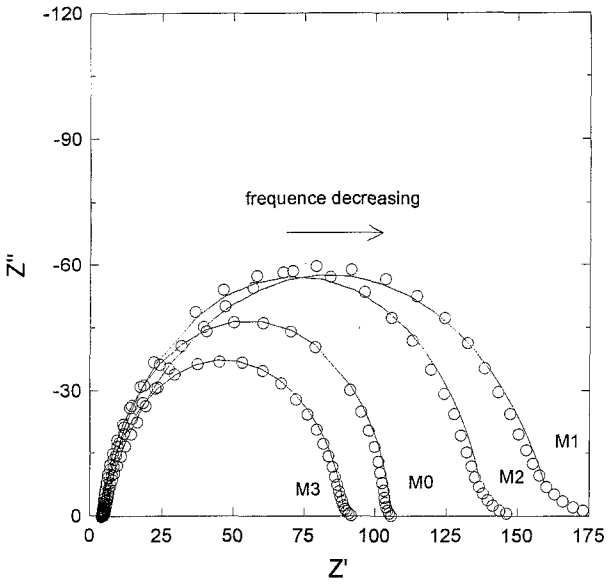

Fig. 5. Nyquist plots for the experimental results (□) the simulated results (——) for the electrodes at 500 mV (vs Ag/AgCl) in 1 M KOH, 30 °C.

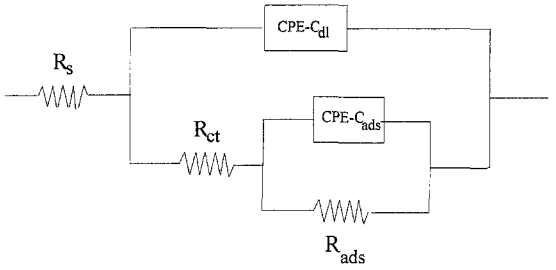

Fig. 6. Equivalent circuit for simulating the a.c. impedance experimental data diagram.

electro-catalytic activity of the M3 electrode is the best at high current density ($j > 10\,mA\,cm^{-2}$). The intensity of Ni(1 1 1)/Ni(2 0 0), 2.92, is much larger than that of the Ni–P electrode (0.11). Consequently, the activity of the M3 electrode is better than that of the Ni–P (M0) electrode. Beside structural characteristics, the electrochemical characteristics of electrodes also depend on particle size (estimated from SEM). Comparing Table 1 and Table 2, the oxygen evolution overpotential and particle sizes are in the same sequence. This indicates that the activity is also affected by true surface area of an electrode. The M3 electrode possesses the largest true surface area (the smallest particle size) and thus its overpotential is the lowest. From the polarization curve of the M0 electrode, the better electrocatalytic activity at low current density is ascribed to the better dispersion of active sites on surface. However, the number of active sites of an electrodes relates not only to active site dispersion but also the surface area of the electrode. At higher current density, the better electrocatalytic activity of the M3 electrode can be deduced from the larger surface area and the ratio of Ni(1 1 1)/Ni(2 0 0).

The ratio of anodic peak charge (Q_a) to cathodic peak charge (Q_c) represents the reversibility of active sites [30]. A Q_c/Q_a value of unity indicates that all active sites return to their original state after the electrolysis process. At least three different forms of nickel oxyhydroxide have been proposed, as identified by either spectrometry [32] or other methods [33, 34]. Previous studies [32, 35] indicated that certain forms of the oxides were irreversible after oxygen evolution. The ratios of Q_c/Q_a for all electrodes of this work are smaller than unity, as indicated in Table 2. The M3 electrode having a ratio 0.999 means that the rejuvenation of M3 electrode is better than any other electrode after undergoing oxygen evolution.

3.2.2. A.c.-impedance analysis. Figure 5 shows the a.c.-impedance results for the electrodes in 1 M KOH solution at a bias potential of 500 mV (vs Ag/AgCl). The potential is selected to facilitate the study on the characteristics of electrodes during oxygen evolution. The results of the Nyquist plots are simulated with a proper equivalent-circuit to obtain the charge transfer resistance (R_{ct}). The impedance behaviour of the electroless Ni–Mo–P electrodes in 1 M KOH solution can be simulated by the circuit model shown in Fig. 6. The parallel RC (resistance and capacitance) which is in series with R_{ct} is ascribed to the adsorption [36]. Adsorption is observed only at low Mo content (M0 and M1 electrodes), as indicated in Table 3 in which the parameters used in simulation are listed. In spite that the adsorption term is not negligible in modelling process for the M0 and M1 electrodes, most of the reaction resistance comes from charge transfer process. Among the electrodes, the M3 electrode has the minimum R_{ct}. R_{ct} first increases by introduction of Mo component for example, for M1 as well as M2, and then decreases at the M3 electrode. In the oxygen evolution region (~500 mV vs Ag/AgCl), R_{ct} of the Ni–Mo–P (M3) electrode is close to that of Ni–P (M0) and the R_{ct} values of M0 and M3 are smaller than those of the M1 and M2 electrodes. The sequences of oxygen overpotential for the electrodes at

Table 3. A.c.-impedance analysis results

Electrode	R_{ct} /Ω cm^2	R_{ads} /Ω cm^2	C_{dl} /mF cm^{-2}	C_{ads} /mF cm^{-2}	$1/(R_{ct}\,Q_a)$ /Ω mC cm^2
M0	50	0.71	1.21	1.92×10^{-1}	1.24×10^{-3}
M1	64	0.38	3.19	1.16×10^{-3}	2.32×10^{-3}
M2	62	0	1.74	0	2.96×10^{-3}
M3	43	0	2.39	0	4.73×10^{-3}

higher current density region (100 mA cm^{-2}) and the charge transfer resistance at 500 mV (vs Ag/AgCl) are the same, M1 > M2 > M0 > M3. For oxygen evolution on the Ni–Mo–P electrodes, the charge transfer resistance is ascribed to the transformation of oxyhydroxide to higher state oxide (NiO_2), and the reaction occurs at ~500 mV (vs Ag/AgCl). The inverse of R_{ct}, $1/R_{ct}$, which is proportional to the product of the number of active sites and the site activity represents the electrocatalytic activity in kinetic control region. The electrochemical activity ($1/R_{ct}$) is used to evaluate the performance of an electrode [37, 38]. The activity of a single site is also an important index of the performance of an electrode. The site activity can be evaluated by the value of $1/R_{ct}Q_a$ [36, 37], as presented in Table 3. $1/R_{ct}Q_a$ increases with molybdenum content. The introduction of molybdenum improves the site activity of the electrode as is the case with the ratio of Ni(1 1 1)/Ni(2 0 0). It is found that the larger the ratio of Ni(1 1 1)/Ni(2 0 0), the better the site activity. Consequently, when an electroless nickel electrode is prepared with a larger amount of Ni(1 1 1), its performance is improved. However, the activity of electrode relates not only to the site activity but also the site number. The site activities of the M1 and the M2 electrode are better than the M0 electrode, but their active site numbers are much smaller than the M0. In summary, the electrocatalytic activities of the M1 and the M2 electrodes are smaller than that of the M0 electrode due to smaller site numbers on the M1 and M2. Both the site activity and the active site number of the M3 electrode are the largest among the electrodes, its electrocatalytic activity is consequently the best. Electrochemical characteristics of the electroless Ni–Mo–P electrodes are discussed in the next section.

3.2.3. Characterization of the electroless Ni–Mo–P electrodes from kinetic model. The mechanisms of oxygen evolution on electroless Ni–Mo–P electrodes are suggested as being the same as those on nickel in alkaline solution [6, 34]:

$$\mathrm{Ni(III)OOH} + \mathrm{OH^-} \xrightarrow[\text{r.d.s}]{k_1(E)} \mathrm{Ni(IV)O_2} + \mathrm{H_2O} + \mathrm{e^-} \quad (1)$$

$$\mathrm{NiO_2} + \mathrm{H_2O} \xrightarrow{k'_{c1}} \mathrm{NiOOH\cdots OH} \quad (2)$$

$$\mathrm{NiOOH\cdots OH} + \mathrm{NiO_2} \xrightarrow{k'_{c2}} \mathrm{NiOOH\cdots O} + \mathrm{NiOOH} \quad (3)$$

$$\mathrm{2NiOOH\cdots O} \xrightarrow{k'_{c3}} \mathrm{2NiOOH} + \mathrm{O_2} \quad (4)$$

NiOOH is electrooxidized to NiO_2 through an electrochemical reaction (Equation 1). NiO_2 reacts with water to evolve oxygen and then reduces to NiOOH simultaneously through chemical reactions (Equations 2–4).

Based on this reaction scheme with Reaction 1 as the rate determining step, a kinetic equation has been developed in our previous study [6]. The derived

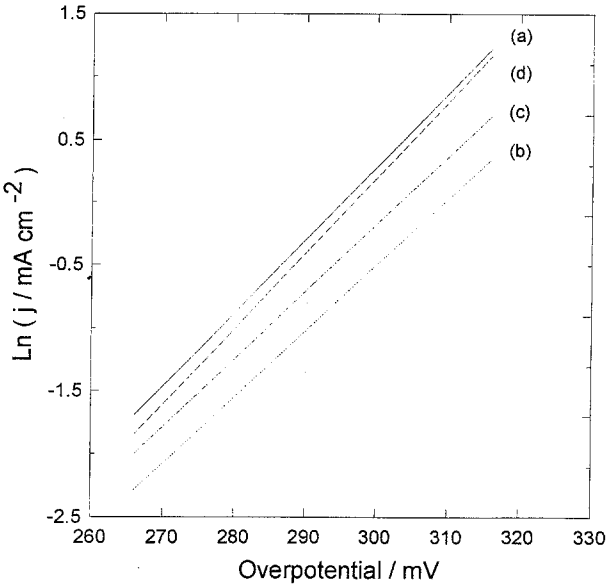

Fig. 7. Plots of ln$j$ against potential for the electroless Ni–Mo–P electrodes: (a) M0, (b) M1, (c) M2, (d) M3.

rate equation is

$$j = 2Fk_1k_{c1}/(k_1 + 2k_{c1}) \quad (5)$$

with

$$k_1 = k'_1\gamma C_{OH^-} = k_{10}\exp(b'\eta), \qquad b' = \alpha F/RT \quad (6)$$

The larger the b' value, the less overpotential is required for oxygen evolution. Since Reaction 1 is a rate determining step, for which $k_1 \ll k_{c1}$ in the region of small overpotential, Equation 5 is simplified as

$$j = Fk_1 \quad (7)$$

Taking natural logarithm of Equation 7

$$\ln j = \ln(Fk_{10}) + b'\eta \quad (8)$$

Therefore, the relationship ln$j$ and η is linear and b' can thus be obtained from Equation 8. By comparison with the experimental data, rate constants, k_{10}, as well as k_{c1}, are derived over a whole range of potential

$$\frac{F}{j} = \frac{1}{k_{10}}\exp(-b'\eta) + \frac{1}{2k_{c1}} \quad (9)$$

Figure 7 shows the relationship between ln$j$ and the overpotential for oxygen evolution on the electroless Ni–P and Ni–Mo–P electrodes in 1 M KOH in the low overpotential regime, b' for each electrode were estimated from comparison of Equation 8 and Fig. 7. Once b' were obtained, k_{c1} and k_{10} can be estimated via a plot of $1/j$ against $\exp(b'\eta)$ and Equation 9. The plots of $1/j$ against $\exp(b'\eta)$ are illustrated in Fig. 8. The values b', k_{10} and k_{c1} as derived are reported in Table 4. Tafel slopes (b) were also estimated and the results are summarized in Table 4 for the electrodes prepared in various Mo-complex concentrations. b' decreases with introduction of Mo component and then increases at the M3 electrode. Since b' represents the efficiency of NiOOH transform-

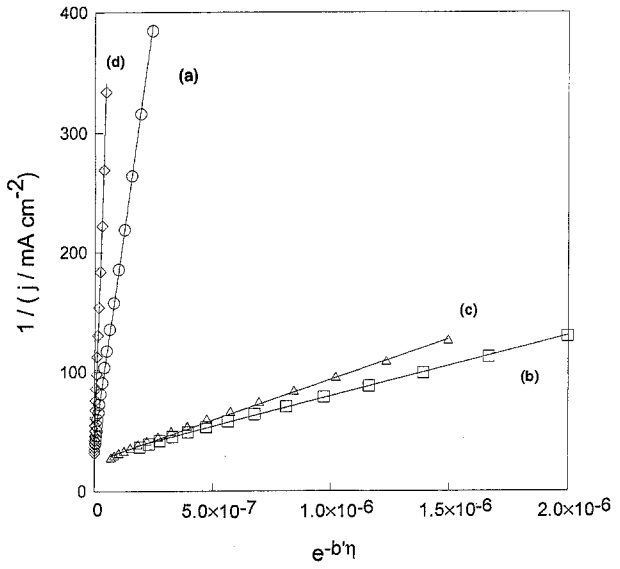

Fig. 8. Plots of $1/j$ against $\exp(-b'\eta)$ for the electrodes Ni–Mo–P electrodes: (a) M0, (b) M1, (c) M2, (d) M3.

Table 4. Some electrochemical parameters evaluated from the kinetic model

Electrode	k_{10}/ mol cm^{-2} s^{-1}	k_{cl}/ mol cm^{-2} s^{-1}	b/ mV dec^{-1}	b'/ mV^{-1}
M0	1.65×10^{-11}	1.18×10^{-2}	40.8	0.0583
M1	2.55×10^{-10}	1.15×10^{-2}	46.2	0.0527
M2	1.75×10^{-10}	1.89×10^{-2}	44.3	0.0539
M3	1.01×10^{-12}	5.71×10^{-3}	38.2	0.0603

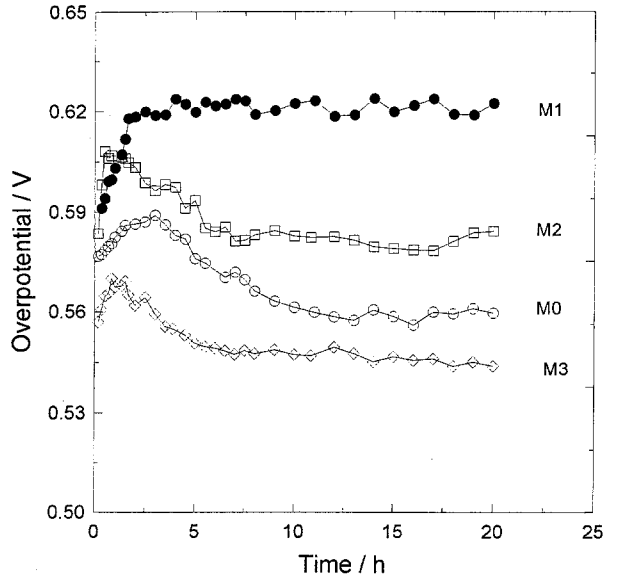

Fig. 9. Prolonged polarization for the electrode at $j = 100\,\text{mA cm}^{-2}$, 30 °C.

ing to a higher value oxide (NiO_2), the electrode with larger b' is expected to possess better electrocatalytic activity. The b' value, and thus the electrochemical conversion efficiency of NiOOH to NiO_2 on the M3 electrode is the largest. Next to the M3 electrode is the Ni–P electrode. However, its site activity and ratio of Ni(1 1 1)/Ni(2 0 0) are the smallest. This phenomenon may raise from the amorphous-like structure of the electroless Ni–P. The structure of the Ni–P electrode is amorphous, as indicated by XRD, but from an AFM study of [6], the micromorphology showed small particles with orientation. Active sites are more uniformly distributed on the Ni–P electrode which may be the main reason for the larger b' value. All the experimental data, oxygen overpotential at $100\,\text{mA cm}^{-2}$, R_{ct} at 500 mV and the b' value, lead to the same finding that the electrocatalytic activity of the M3 electrode is better than that of any other electrode in this work. The electrocatalytic activity of the M3 electrode increases as a result of increase of both site activity and surface area. The Tafel slopes of the electrodes were found to be within the range 43–46 mV dec^{-1}. These values are smaller than those for Raney nickel (50–80 mV dec^{-1}) [39] but are approximately equal to those for IrO_2 (40–50 mV dec^{-1}) [2]. From the above analysis, the Ni–Mo–P electrodes prepared by electroless deposition have considerable promise for use in oxygen evolution and may also be suitable for organic oxidation. The prolonged galvanostatic experiments at $100\,\text{mA cm}^{-2}$ were carried out to explore the stability of the Ni–Mo–P electrodes, as shown in Fig. 9. This indicates that all the electrodes are stable over the period studied; however, the M3 electrode shows better activity than the other electrodes.

Acknowledgement

The authors wish to thank the National Science Council (NSC 83-0416-E-011-002) of the R.O.C. for financial support and National Taiwan Institute of Technology of the Republic of China.

References

[1] B. E. Conway, M. A. Sattar and D. Gilroy, *Electrochim. Acta* **14** (1969) 677.
[2] H. J. Miao and D. L. Piron, *J. Appl. Electrochem.* **21** (1991) 55.
[3] J. L. Weininger and M. W. Breiter, *J. Electrochem. Soc.* **111** (1964) 707.
[4] M. H. Miles, G. Kissel, P. W. T. Lu and S. Srinivasan, *ibid.* **123** (1976) 332.
[5] M. H. Miles, *J. Electroanal. Chem.* **60** (1975) 89.
[6] Y. L. Lo and B. J. Hwang, *J.Ch.I.Ch.E*, submitted.
[7] G. Vétes and G. Horányi, *J. Electroanal. Chem.* **52** (1974) 47.
[8] M. Fleischmann, K. Korinek and D. Pletcher, *ibid.* **31** (1971) 39.
[9] P. M. Robertson, *ibid.* **111** (1980) 97.
[10] M. Amjad, D. Pletcher and C. Smith, *J. Electrochem. Soc.* **124** (1977) 203.
[11] Y. L. Lo and B. J. Hwang, *ibid.* **142** (1995) 445.
[12] G. O. Mallory, *Plat. Surf. Finish.* **63** (1976) 34.
[13] I. Koiwa, M. Nishikawa, K. Yamada and T. Osaka, *Bull. Chem. Soc. Jpn.* **59** (1986) 133.
[14] Y. L. Lo and B. J. Hwang, *Ind. Eng. Chem. Res.* **33** (1994) 56.
[15] A. K. Misra, *J. Electrochem. Soc.* **133** (1986) 1029.
[16] A. P. Brown, *ibid.* **134** (1987) 1921.
[17] K. Ravi, V. Ramaswamy and T. K. G. Namboodhiri, *Mater. Sci. Eng.*, **A169** (1993) 111.
[18] G. O. Mallory and T. R. Horhn, *Plat. Surf. Finish.* **66** (1979) 40.
[19] I. Kowia, M. Usuda, K. Yamada and T. Osaka, *J. Electrochem. Soc.* **135** (1988) 718.
[20] T. Osaka, H. Yamazaki, I. Saito and J. Kawaguchi, *ibid.* **136** (1989) 3418.

[21] C. Fan, D. L. Piron, A. Sleb and P. Paradis, *J. Electrochem. Soc.* **141** (1994) 382.
[22] I. A. Raj and K. I. Vasu, *J. Appl. Electrochem.* **20** (1990) 32.
[23] J. Divisek, H. Schmitz and J. Balej, *ibid.* **19** (1989) 519.
[24] J. Y. Huot, M. L. Trudeau and R. Schulz, *J. Electrochem. Soc.* **138** (1991) 1316.
[25] L. B. Albertini, A. C. D. Angleo and E. R. Gonzalez, *J. Appl. Electrochem.* **22** (1992) 888.
[26] P. N. Pintauro, N. Phan, M. M. Baizer and K. Nobe, *in* 'AIChE Symposium Series', American Institute of Chemical Engineers (1987) vol. **83**, p.34.
[27] B. D. Cullity, 'Elements of X-ray Diffraction', 2nd ed., Addison-Wesley, London (1978) p. 102.
[28] A. J. Bard (ed.) 'Encyclopedia of Electrochemistry of the Elements', vol. 3, Marcel Dekker, New York (1975) p. 331.
[29] H. Alemu and K. Jüttner, *Electrochim. Acta* **33** (1988) 1101.
[30] R. S. S. Guzmán, J. R. Vilche and A. J. Arvia, *J. Electrochem. Soc.* **125** (1978) 1578.
[31] L. Varcar and B. E. Conway, *Electrochim. Acta* **35** (1990) 1919.
[32] C. Zhang and S.-M. Park, *J. Electrochem. Soc.* **136** (1989) 3333.
[33] J. L. Weininger and M. W. Breiter, *ibid.* **110** (1963) 484.
[34] R. E. White, J. O'M. Bockris and B. E. Conway, 'Modern Aspects of Electrochemistry', No. 21, Plenum Press, New York (1990) p. 47.
[35] D. M. Mac Arthur, *J. Electrochem. Soc.* **117** (1970) 422.
[36] C. M. A. Brett and A. M. O. Brett, 'Electrochemistry Principles, Methods, and Applications', Oxford University Press, New York (1993) p. 245.
[37] B. J. Hwang, D. T. Shieh and A. S. T. Chang, *J. ChIChE* **25** (1994) 127.
[38] D. T. Sheih and B. J. Hwang, *ibid.* **25** (1994) 87.
[39] L. Brossard and C. Messier, *J. Appl. Electrochem.* **23** (1993) 379.